Thirty years of in situ stratospheric aerosol size distribution measurements from Laramie, Wyoming (41°N), using balloon-borne instruments

T. Deshler,[1] M. E. Hervig,[2] D. J. Hofmann,[3] J. M. Rosen,[4] and J. B. Liley[5]

Received 8 May 2002; revised 16 August 2002; accepted 2 October 2002; published 13 March 2003.

[1] Vertical profiles of size-resolved aerosol concentrations above Laramie, Wyoming (41°N), have been measured for the past thirty years, 1971-2001. During this period, two somewhat different optical particle counters have been used to measure particles with radii $\geq$0.15 μm, whereas the instrument to measure condensation nuclei (CN) has not changed significantly since the late 1970s. The two optical particle counters measure aerosols $\geq$0.15, 0.25 μm and aerosols $\geq$0.15–2.0 μm in twelve size classes. These measurements have concentration (N) uncertainties $\propto \pm N^{-0.5}$, but with a minimum of ±10%. Sizing uncertainties are about ±10%. The impact of these uncertainties on size distribution fitting parameters and aerosol moments are approximately ±30% and ±40%. The long-term record from these measurements indicates that volcanoes have controlled stratospheric aerosol abundance for 20 of the past 30 years. The present period, beginning in 1997, represents the longest volcanically quiescent period in the record. These and other measurements clearly show that stratospheric aerosol are now in a background state, a state rarely occurring in recent times, and that this background state is not significantly different than observations in 1979. Aerosol volumes and surface areas, inferred from size distributions fit to the measurements, are compared with SAGE II satellite estimates of surface area and volume. For volume the measurements are in agreement within measurement error throughout the record. For surface area there is good agreement for a volcanic aerosol laden stratosphere, but for background aerosol conditions the SAGE II estimates are about 40% less than the in situ measurements. Present aerosol surface areas are ~1.0 (0.6) μm^2 cm^{-3} in the 15–20 (20–25) km layer based on in situ measurements. The Laramie size distribution record is now available to the community over the internet. *INDEX TERMS:* 0305 Atmospheric Composition and Structure: Aerosols and particles (0345, 4801); 0340 Atmospheric Composition and Structure: Middle atmosphere—composition and chemistry; 0370 Atmospheric Composition and Structure: Volcanic effects (8409); *KEYWORDS:* stratospheric aerosol size distributions, volcanic stratospheric aerosol, background stratospheric aerosol, in situ aerosol size distribution measurements, optical particle counters, balloonborne aerosol measurements

Citation: Deshler, T., M. E. Hervig, D. J. Hofmann, J. M. Rosen, and J. B. Liley, Thirty years of in situ stratospheric aerosol size distribution measurements from Laramie, Wyoming (41°N), using balloon-borne instruments, *J. Geophys. Res.*, *108*(D5), 4167, doi:10.1029/2002JD002514, 2003.

1. Introduction

[2] The stratospheric aerosol layer was first measured in the late 1950s using balloon-borne impactors [*Junge et al.*, 1961] and is often called the Junge layer, although its existence was suggested 50 years earlier from twilight observations [*Gruner and Kleinert*, 1927]. *Junge et al.*'s [1961] measurements were at the end of an extended volcanic-free period [*Stothers*, 1996], but were not extensive enough to establish a baseline for stratospheric aerosol. Estimates of the global stratospheric aerosol burden, and clarifying the source of the sulfuric acid, had to wait for long-term measurements which began in the early 1970s using lidar [*Jäger*, 1991; *Osborn et al.*, 1995; *DeFoor et al.*, 1992]; balloon-borne particle counters [*Hofmann et al.*, 1975; *Hofmann and Rosen*, 1980; *Hofmann*, 1990]; and in the late 1970s satellite instruments: SAM (Stratospheric Aerosol Measurements) II (1979–1991) [*Pepin et al.*, 1977; *Poole and Pitts*, 1994], SAGE (1979–1981) (Stratospheric Aerosol and Gas Experiment) and SAGE II (1984–present) [*McCormick et al.*, 1979]. The importance of

[1]Department of Atmospheric Science, University of Wyoming, Laramie, Wyoming, USA.
[2]G & A Technical Software (GATS) Inc., Driggs, Idaho, USA.
[3]National Oceanic and Atmospheric Administration, Boulder, Colorado, USA.
[4]Department of Physics and Astronomy, University of Wyoming, Laramie, Wyoming, USA.
[5]National Institute of Water and Atmospheric Research, Lauder, New Zealand.

0148-0227/03/2002JD002514$09.00

volcanic eruptions then became clear, and these have been shown to be the dominant source of aerosol in the past 30 years. Comparing the last 30 years with the previous 100 years suggests that the most recent period can be characterized as a relatively active volcanic period. Through primarily the use of historical solar and stellar extinction data, *Sato et al.* [1993] and *Stothers* [1996] show that the past 100 years have been dominated by eight major eruptions. Four of these occurred between 1880 and 1910 and four since 1960. Since 1970, there have been three major volcanic perturbations to stratospheric aerosol: Fuego (14°N, October 1974, 3–6 MT), El Chichón (17°N, April 1982, 12 MT), and Pinatubo (15°N, June 1991, 30 MT) [*McCormick et al.*, 1995]. Within this record there have been 4 periods, 1974, 1979, 1989–1990, and 1997–present when the influence of volcanic eruptions was at a minimum.

[3] Stratospheric aerosol plays a role in a number of processes affecting the global chemical and radiation balance of the atmosphere [*McCormick et al.*, 1995; *Solomon*, 1999]. During periods of high aerosol load there is evidence for enhanced ozone loss through heterogeneous chemistry [*Angell et al.*, 1985; *Hofmann and Solomon*, 1989; *Jäger and Wege*, 1990; *Gleason et al.*, 1993; *Deshler et al.*, 1996], stratospheric warming [*Labitzke and McCormick*, 1992; *Angell*, 1993; *Russell et al.*, 1993], and tropospheric cooling [*Dutton and Christy*, 1992]. During long volcanically quiescent periods, when stratospheric aerosol can be characterized as in a background state unperturbed by volcanism, radiative effects of stratospheric aerosol are minimized, but these aerosol still play an important role for a number of trace gases. In particular, NO_x is sensitive to aerosol loading. Reductions in NO_2 columns were observed after both El Chichón and Pinatubo [*Johnston and McKenzie*, 1989; *Johnston et al.*, 1992]. These reductions result from the hydrolysis of N_2O_5 on water bearing volcanic sulfuric acid aerosol [*Rowland et al.*, 1986; *Tolbert et al.*, 1988; *Mozurkiewicz and Calvert*, 1988]. At low aerosol loading, NO_x is increased and plays a role in the ozone budget. *Fahey et al.* [1993] provided direct measurements of anticorrelation of aerosol surface area and the NO_x/NO_y ratio. Because hydrolysis of N_2O_5 saturates as aerosol surface area increases above 5–10 μm^2 cm^{-3}, the role aerosol play in controlling NO_x is much more critical during periods of low aerosol loading [*Prather*, 1992]. *Fish et al.* [2000] demonstrate the impact of a 20% reduction in satellite observed aerosol on modeled trends of NO_2 in the southern hemisphere. Increases in NO_x imply larger ozone loss from the nitrogen catalytic cycle [*Crutzen*, 1970]. Changes in NO_x also have direct implications for the abundance of ClO_x and HO_x, both of which also have a direct bearing on ozone in midlatitudes [*Wennberg et al.*, 1994; *Solomon et al.*, 1996]. The importance of aerosol surface areas in stratospheric chemistry has only been fully realized in the past fifteen years beginning with *Solomon et al.* [1986]. Long-term stratospheric aerosol measurements had their beginnings about fifteen years prior to this realization. The impact of stratospheric aerosol on chemistry has led to a renewed interest in these measurements beyond their role in characterizing volcanic perturbations of the stratosphere and the evolution of the particles produced. In situ measurements from Laramie, Wyoming (41°N), began in 1971, slightly preceding long-term lidar measurements from Garmisch-Partenkirchen, Germany (47°N); Hampton, Virginia (37°N); and Mauna Loa, Hawaii (20°N) [*Jäger*, 1991; *Osborn et al.*, 1995; *Barnes and Hofmann*, 1997].

[4] Measurements in the 1970s and 1980s from Laramie established: the boiling point of stratospheric aerosol [*Rosen*, 1971]; the first stratospheric profiles of CN [*Rosen and Hofmann*, 1977]; the composition of stratospheric aerosol [*Hofmann and Rosen*, 1984]; the effect of the Fuego, Alaid, and El Chichón volcanic eruptions [*Hofmann and Rosen*, 1981a, 1981b; *Hofmann and Rosen*, 1983; *Hofmann and Rosen*, 1987]; and contributed to the validation of satellite instruments [*Russell et al.*, 1981, 1984; *Wang et al.*, 1989]. Measurements in the 1990s have been strongly influenced by the eruption of Pinatubo in 1991. Since Pinatubo, aerosol measurements at Laramie have been used by numerous investigators: to validate Upper Atmospheric Research Satellite measurements [*Massie et al.*, 1996a; *Lambert et al.*, 1996; *Hervig et al.*, 1996]; to study the distribution and evolution of Pinatubo aerosol using both satellite and in situ measurements [*Grainger et al.*, 1995; *Massie et al.*, 1996b]; to compare with a global climatology of stratospheric aerosol surface areas from SAGE II [*Thomason et al.*, 1997b; *Hervig and Deshler*, 2002]; to contribute to a broad data set presenting the global to microscale evolution of Pinatubo volcanic aerosol [*Russell et al.*, 1996]; to contribute to the development of a climatology for stratospheric aerosol effects on ultraviolet radiation [*Stevermer et al.*, 2000]; and to develop a method for inferring aerosol size distributions from Halogen Occultation Experiment (HALOE) data [*Hervig et al.*, 1998].

[5] Volcanic events have been the primary focus of these analyses because background periods have been more elusive. There have, however, been some analyses of the measurements just prior to the three major eruptions of the past thirty years. One of the first of these [*Hofmann and Rosen*, 1980; *Hofmann and Rosen*, 1981a] compared the pre-Fuego and pre-El Chichón periods. Although the former period was too short to establish a background, it was similar to the much longer pre-El Chichón period. Comparison of these measurements with initial measurements of *Junge et al.* [1961], which were at the end of an extensive volcanic-free period, suggested a possible increase of about of factor of 5–6 in aerosol concentration at 20 km during the intervening 20 years [*Hofmann and Rosen*, 1980]. This problem was revisited by *Hofmann* [1990], who compared measurements of aerosol mixing ratio for 0.15 and 0.25 μm radius thresholds during volcanically unperturbed periods in 1974, 1979, and 1989. Although no change was observed in the mixing ratio of 0.15 μm particles, there was about a 50% increase in mixing ratio of particles >.25 μm between 1979 and 1989. Based on these changes Hofmann estimated an increase in aerosol mass on the order of 5% yr^{-1} over the decade. *Thomason et al.* [1997a] noticed a similar increase based on SAGE II measurements, but suggested that 1989 may not have been at true background, due primarily to Nevado del Ruiz in 1985, and thus the elevated aerosol observed may be due to residual volcanic aerosol. Resolution of the questions raised by these studies had to wait for the third background period in the modern record, the present, when the decay of El Chichón and Pinatubo aerosol could be compared. *Barnes and Hofmann* [1997], using long-term lidar measurements at Mauna Loa, Hawaii,

showed that the decay of aerosol loading following El Chichón and Pinatubo was influenced by the phase of the quasi-biennial oscillation (QBO) in tropical stratospheric winds. They also presented measurements of integrated aerosol backscatter in 1995 which were below any previous observations at Mauna Loa. Another comparison of the pre-Pinatubo and post-Pinatubo periods was performed by *Hayashida and Horikawa* [2001] using SAGE II extinction measurements to derive Ångström parameters. They conclude that the pre-Pinatubo period was still influenced by volcanic eruptions from the mid 1980s and cannot be considered a real background period. *Barnes and Hofmann* [2001] have used the present background period, extending from 1996, to demonstrate variability correlated with the phase of the QBO, with implications for the source of these background particles.

[6] The purpose of this paper is to bring the Laramie record up to date in terms of instruments used, errors associated with measurements and fitting algorithms, measurements available, and comparisons with other long-term records, notably SAGE II.

2. Instrument Description

[7] Stratospheric aerosol measurements at Laramie, Wyoming, began in 1971 using the University of Wyoming optical particle counter (OPC), which was initially developed by *Rosen* [1964]. The instrument is a white light counter measuring aerosol scattering at 25° in the forward direction and using Mie theory to determine aerosol size. An incandescent lamp and light controller supply constant illumination of the scattering region. The incandescent lamp filament, imaged in the scattering region, is larger than the aerosol sample stream, thus edge effects are not a problem in defining sample volume. Light scattered from particles passing through the beam is collected over a solid angle of ~30° and focused onto a photomultiplier tube (PMT) for pulse height detection. Two symmetrical independent photon paths are used to limit noise and the influence of cosmic rays by coincidence counting. Integral particle concentrations are measured by counting coincident PMT pulses which exceed preset discriminator levels. These instruments are sensitive to optically detectable aerosol as small as 0.15 μm in radius. Initial measurements in the 1970s consisted of measurements of particles >0.15 and 0.25 μm at a sample flow rate of 1 L min^{-1}. These instruments have been referred to as dustsondes in the past, but here we refer to them as OPC25s reflecting an OPC with scattering angle centered at 25°.

[8] In the late 1970s a similar instrument was coupled with a chamber to supersaturate the sampled air stream with ethylene glycol vapor. By growing all particles > 0.01 μm in the sample stream to optical detection thresholds, this combination measures condensation nuclei (CN) concentrations [*Rosen and Hofmann*, 1977; *Rosen et al.*, 1978]. The saturation chamber consists of a heated cylinder whose walls are coated with ethylene glycol. The condensing chamber, following the saturation region, is held at 0°C. The magnitude and duration of the supersaturation region in the condensing chamber is a function of pressure, decreasing from saturation ratios as large as 2 near the Earth's surface to less than 1.5 above 50 mbar. The temperature of the saturation chamber is increased at low pressures to maintain adequate supersaturations. Rough counting efficiency tests indicated that the instrument is quite sensitive to particles <0.01 μm at pressures as low as 40 mbar [*Rozier*, 1993].

[9] An additional instrument was developed in the early 1980s to measure low concentrations of large particles produced by the volcanic eruptions of Mt. St. Helens and El Chichón [*Hofmann and Rosen*, 1982]. This required enlarging the scattering chamber and adding a 50 L min^{-1} pump, but maintaining the same scattering angle. These large-particle counters were flown through 1987 in conjunction with OPC25s, but measurements were limited to particles <0.4 and >1.0 μm by ambiguity of instrument response over the intervening region in both the OPC25 and the 50 L min^{-1} instrument.

[10] In 1989 the OPC25 design was modified to make measurements in the ambiguous region, to increase the number of sizes measured, and to decrease minimum concentrations measurable. This development began in response to the need for in situ measurements of polar stratospheric cloud particles >0.4 μm. The scattering angle of the detector axis was increased from 25 to 40° and flow rate increased from 1 to 10 L min^{-1}, with appropriate changes in inlet design to accommodate higher flow rate. This new scattering angle allowed, for the first time, unambiguous detection of particles throughout the size range 0.15–10.0 μm. The number of sizes measured was increased to eight and then twelve channels. The new instrument is now capable of providing measurements of particles with radii >0.15 μm in twelve size classes. The upper channel is determined based on application, but typically varies between 2.0 μm for midlatitude measurements and 10.0 μm for polar stratospheric cloud measurements. Minimum detectable concentrations for this instrument are 6×10^{-4} cm^{-3} as opposed to 6×10^{-3} cm^{-3} for the OPC25. These OPCs, hereafter referred to as OPC40, were first used in Antarctica in September 1989 [*Hofmann and Deshler*, 1991]. After calibration flights in Laramie to insure that the lower sizes measured with this new instrument were in agreement with the OPC25, the new instrument has replaced the earlier instrument for flights in Laramie as well. Current measurement capabilities consist of CN and optically detectable aerosol, $r \geq 0.15$–2.0 or 10.0 μm in twelve size ranges, from the surface to 30 km. The complete history of the aerosol sizes measured at Laramie is listed in Table 1.

[11] Theoretical counter response curves for both the OPC25 and OPC40 are calculated from

$$CR = \int_{\Theta - cl_2}^{\Theta + cl_2} \mathrm{cl}(\phi)\, d\phi \int_{\phi - fl_2}^{\phi + fl_2} \mathrm{fl}(\phi, \theta)\, d\theta \cdot \int_{0.3\mu\,\mathrm{m}}^{0.7\mu\,\mathrm{m}} \left(\frac{\lambda}{2\pi}\right)^2 [\mathbf{i}_1(x, m, \theta) + \mathbf{i}_2(x, m, \theta)] \cdot \mathbf{I}(\lambda)\mathrm{QE}(\lambda)\, d\lambda. \quad (1)$$

Functions *cl* and *fl* describe the optical counter light collection efficiency as a function of angle from the forward scattering direction, centered at Θ, for the optical geometry of the scattering chamber, Figure 1. The half angles subtended by the lens focusing the filament onto the scattering region and the lens collecting scattered light are fl_2 and cl_2. The integration over wavelength, λ, is limited to the quantum efficiency for the PMTs used, QE. The bracketed terms are the Mie scattering efficiency for particles

Table 1. History of Aerosol Sizes Measured Using OPCs Flown From Laramie, Wyoming

Begin	End	Aerosol Sizes Measured, μm
Jan 1971	Jun 1982	0.15 0.25
Jun 1982	Dec 1987	0.15 0.25 0.95 1.20 1.80, two instruments
Jan 1988	Apr 1989	0.15 0.25
May 1989	Nov 1989	0.15 0.25 0.5 1.0 2.0 3 5 10
Dec 1989	Feb 1990	0.15 0.25
Mar 1990	Aug 1990	0.15 0.25 0.5 1.0 2.0 3 5 10
Sep 1990	Mar 1991	0.15 0.25
Mar 1991	Apr 1992	0.15 0.25 0.5 1.0 2.0 3 5 10
May 1992	Nov 1993	0.15 0.25 0.5 0.75 1.0 1.08 1.45 2.0
Nov 1993	Present	0.15 0.19 0.25 0.30 0.38 0.49 0.62 0.78 1.08 1.25 1.58 2.0

with index of refraction, m, size parameter, $x = 2\pi r/\lambda$, and scattering angle θ. Intensity of the light source, I, is given by the Planck function for a blackbody temperature of 3300 K. The calculation above is not absolute and must be normalized by matching theoretical counter response to a measured response for particles of known index of refraction and size. Calibration at a single particle size is sufficient. Similar calculations have been previously described by, for example, *Pinnick et al.* [1973] and *Quenzel* [1969].

[12] All of the aerosol counters are calibrated in the same way. Monodisperse aerosol particles are sampled, and instrument gain is adjusted until measured instrument response is consistent with theoretical instrument response for the size of particles used. Typically instruments are calibrated using commercially available polystyrene latex (PSL) spheres near 0.5 μm radius. This standard aerosol has been used since the 1970s. Although it is sufficient to calibrate the instrument using only one particle size, the theoretical counter response curve has been checked a number of times using monodisperse particles of several sizes and compositions (refractive indices). Early comparisons of measured and calculated instrument response for an OPC25 using nigrosin dye, ink, Dow Corning 200 fluid, and PSL were completed by *Pinnick et al.* [1973]. More recently, we have made similar comparisons of the response of an OPC25 and OPC40 to monodisperse samples of NaCl, diethyl hexyl sebacate (DES), and PSL [*Zhao*, 1996; *Miao*, 2001].

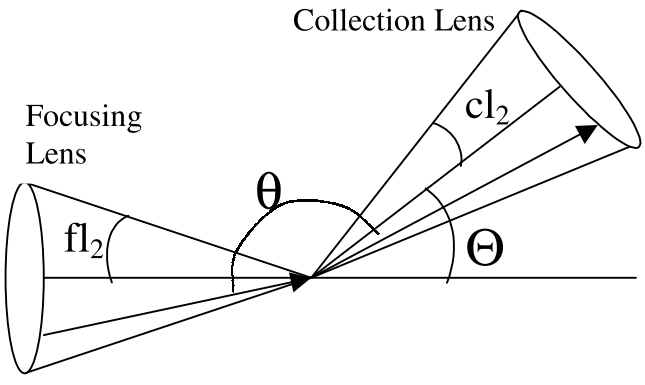

Figure 1. Schematic of the optical configuration of the University of Wyoming optical particle counter. Photons scattered into the detector behind the collection lens can originate anywhere along the focusing lens. The arrows illustrate a possible photon path.

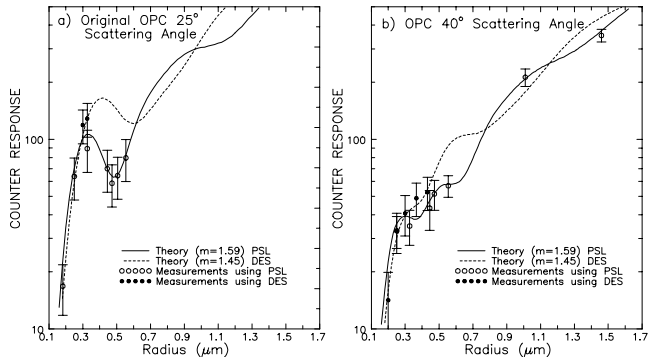

Figure 2. Counter response for the Wyoming OPCs at two indices of refraction compared with measurements on monodisperse polystyrene latex spheres (PSL) and diethyl hexyl sebacate (DES). (a) Counter response for a counter with photodetectors centered at 25° in the forward direction, OPC25. (b) As in (a) but with detectors centered at 40°, OPC40.

[13] Theoretical counter response curves compare well to measurements on PSL and DES for an OPC25 and an OPC40, Figure 2 [*Zhao*, 1996]. Error bars on the measured counter response represent full width at half maximum pulse height for a population of monodisperse particles passing through the beam. For monodisperse aerosol, deviation of measured pulse height distributions from an ideal delta function quantifies sizing error. Deviations result primarily from variations in PMT responsiveness for a constant optical input. Variations in intensity of the light beam, and variations in aerosol paths through the beam play a secondary role. Variations in particle size for the monodisperse samples used do not contribute significantly to the error budget. The PSL spheres were checked in the early 1990s using electron microscopy and found to have a standard deviation of 0.015 μm, ~1% (P. Sheridan, personal communication, 1992). The DES aerosol were created using a differential mobility analyzer and have a similar standard deviation.

[14] Errors induced by variations in PMT response are a function of pulse height and decrease from 40% at the smallest sizes, 0.15 μm, to about 20% at 0.3 μm and larger. This is based on measurements of PMT response to a constant photo input from a light emitting diode [*Miao*, 2001]. See also *Sugita et al.* [1999], *Pinnick and Hofmann* [1973], and *Oesburg* [1972]. These errors represent the best sizing accuracy that can be achieved with these instruments due to limitations of the PMT response function. The extent to which errors shown in Figure 2 exceed these values represents the influence of other errors mentioned.

[15] For each set of comparisons in Figure 2 there is one point where the peak in the measured distribution and theoretical counter response match exactly. This point represents the calibration aerosol and corresponds to 0.47 μm for these tests. Figure 2 illustrates the dependence of counter response on index of refraction and removal of ambiguous sizing between 0.4 and 0.9 μm in the 25° counter by increasing the center of the scattering region to 40°. The instrument response function is modeled reasonably well.

[16] Pulse width broadening from PMTs, along with the other errors mentioned, will lead to sizing errors which are a function of index of refraction since the shape of the counter

response curve varies with index of refraction. Using error bars displayed in Figure 2 applied to the curve for m = 1.45 leads to sizing errors which are primarily ~±10%, but increase to ±30% near 0.35 and 0.7 μm where the counter response curve is flatter. To circumvent large sizing errors, size thresholds should be set to avoid flat regions in counter response function. This is, of course, only possible if the index of refraction for the particles to be measured is known.

[17] Using a fixed index of refraction (1.45 here) to estimate particle size can lead to a systematic error dependent on the true refractive indices of particles sampled; however, for stratospheric sulfuric acid aerosol in midlatitudes, variations in index of refraction are minor. For temperatures above −65°C and water vapor concentrations near 5 ppmv, the real part of refractive index for sulfuric acid aerosol varies from 1.43 to 1.45, with no absorption [*Steele and Hamill*, 1981; *Russell and Hamill*, 1984]. Variations of index of refraction in this range lead to sizing errors well below those associated with the pulse width broadening discussed above, and do not contribute significantly to the error analysis.

[18] Errors in concentrations measured by these instruments depends on variations in air sample flow rate, Poisson counting statistics, and the reproducibility of a measurement from two identical instruments. The pumps used for these instruments are constant volume gear displacement pumps, which are quite stable. Little variation is observed in pump rotation rates over pressure ranges encountered in the stratosphere. The pump is housed inside the instrument container, and typical temperature variations are on the order of 20°C to −10°C during a flight. Changes in pump efficiency with pressure will be a function of the efficiency of filling the evacuated chamber as outside pressure decreases, thus changing the absolute pressure difference between evacuated chamber and outside air. This function has been measured in a pressure chamber. Pump flow rates are found to decrease by 3% at ambient pressures of 30 mbar and by 13% at 5 mbar [*Miao*, 2001]. Since these variations are less than other uncertainties, no adjustments to concentration measurements are made for measurements at low pressures. Aerosol flow rates are checked prior to and following a flight.

[19] Laboratory tests with two identical counters on several samples of differently sized monodisperse PSL indicate that precision of measurement is limited to ± 10% for relatively high concentrations of aerosol when Poisson counting statistics are not a factor. Poisson counting statistics define the fractional uncertainty of a count as its inverse square root, $C^{-0.5}$ for C counts in one sample, becoming important at low concentrations. The aerosol concentration, N = C S/F for sample frequency, S, and flow rate, F. Thus the Poisson error fraction, in terms of concentration, is $(N\ F/S)^{-0.5}$. For these instruments: S = 0.1 Hz, F = 16.7 $cm^3\ s^{-1}$ for an OPC25 and CN counter, and F = 167 $cm^3\ s^{-1}$ for an OPC40. In the stratosphere these flow rates are reduced to about 80% of these values by temperature differences between outside air and pump. This leads to uncertainties of 85, 25, and 8% for concentrations of 0.01, 0.1, and 1.0 cm^{-3} at the low flow rate and concentrations of 0.001, 0.01, and 0.1 cm^{-3} at the high flow rate. This error dominates at concentrations below 0.1 (0.01) cm^{-3} for the low (high) flow rate instrument. At concentrations higher than these a concentration error of ±10% reflects comparisons of concentration measurements from two instruments using identical aerosol in the laboratory. Example measurements with a CN and OPC40 are shown in Figure 3 for a case of high stratospheric aerosol loading and a recent measurement with low stratospheric aerosol loading. The importance of Poisson counting statistics is clearly observable as aerosol concentrations decrease for larger sizes and at upper altitudes.

3. Comparisons of OPC25 and OPC40

[20] After the eruption of Pinatubo in 1991 an OPC40, developed for polar stratospheric cloud measurements, was used for regular measurements from Laramie, Wyoming. Prior to and subsequent to this time, numerous tests were performed to insure that the two standard sizes employed since measurements began in 1971, 0.15 and 0.25 μm, were reliably reproduced by newer instruments. The initial discriminator level settings at these sizes were set by theory, and then adjusted with results from joint flights of two instruments. Laboratory facilities were not available to produce stable samples at these sizes. Although discriminator level settings which allow the OPC40 to reproduce 0.15 and 0.25 μm OPC25 measurements were established empirically, deviations from theoretically predicted points are minor. The empirically determined points correspond to 0.13 and 0.24 μm in the OPC40 counter response function. All other sizes measured by an OPC40 are based on the theoretical counter response curve.

[21] Fine tuning the OPC25/OPC40 comparison entailed over 30 flights, 1989–1994. The increased aerosol load from the eruption of Pinatubo in June 1991 considerably reduced counting errors associated with OPC25 measurements, thus permitting a better comparison of the two instruments. Table 2 summarizes comparison flights and concentration ratio averages measured at 0.15 and 0.25 μm for 22 flights. The setting for the 0.15 μm channel was stabilized in 1991, but stabilization of the 0.25 μm channel was not complete until 1994, requiring six additional comparisons. Figure 4 presents ratios of measurements from the two instruments at 0.15 and 0.25 μm for the flight in 1994 when the 0.25 μm measurement stabilized, and for a recent check of an OPC40 against an OPC25. The decrease in stability of the ratio with altitude at both 0.15 and 0.25 μm in 1999 is a reflection of relatively low concentrations, near 0.05 (0.01) cm^{-3} for 0.15 (0.25) μm thresholds, leading to uncertainties of ±40% to ±80% for OPC25 concentration measurements. From Figure 4 and Table 2 we conclude that, on average, concentration measurements at 0.15 μm (0.25 μm) with an OPC40 are within ±10% (20%) of similar measurements with an OPC25. These uncertainties should be kept in mind when the history of aerosol mixing ratio at these two size limits is presented.

4. Size Distributions Fit to Cumulative Concentration Measurements

[22] To provide functional size distributions representing the cumulative concentration measurements, data are fit with either unimodal or bimodal lognormal size distributions [*Jäger and Hofmann*, 1991; *Hofmann and Deshler*, 1991; *Deshler et al.*, 1993]. Thus each measurement of

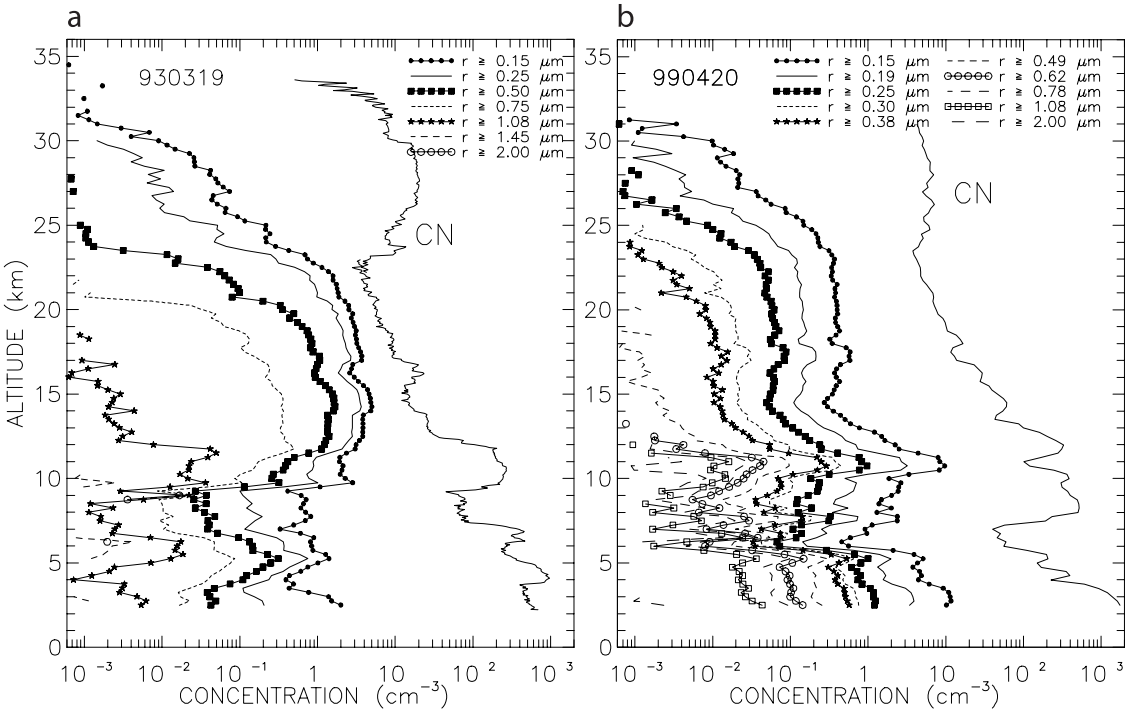

Figure 3. Example aerosol profiles for CN and for aerosol with radius $\geq$0.15 μm. (a) Measurements in 1993, two years after Pinatubo for aerosol with radius $\geq$0.15, 0.25, 0.50,0.75, 1.08, 1.45, 2.0 μm. (b) Measurements in background aerosol in 1999 for aerosol with radius $\geq$ 0.15, 0.19, 0.25, 0.30, 0.38, 0.49, 0.62, 0.78, 1.08, 2.0 μm. The tropopause is at about 11 km on both days.

particle concentration at several discrete size bins is fit with a function of the form

$$N(>r) = \sum_i \int_r^\infty \frac{N_i}{\sqrt{2\pi}\ln\sigma_i} \exp\left(\frac{-\ln^2[a/r_i]}{2\ln^2\sigma_i}\right) d\ln a, \quad (2)$$

where the summation is over either one or two modes of the size distribution. For each mode of the distribution, N_i is total number concentration, r_i median radius, and σ_i distribution width. N(>r) represents the concentration of all particles larger than the lower integration limit, r, and is the quantity measured by the OPCs. The total number concentration, or

Table 2. Summary of Concentration Ratios of 0.15 and 0.25 μm Particles (OPC25/OPC40) for 22 Flights Comparing the OPC25 and OPC40[a]

	Altitude-Interval		Ratio 0.15 μm		Discrm. Level	Ratio 0.25 μm		Discrm. Level
Date	Bot., km	Top, km	Ave.	Std. Dev.	Voltage	Ave.	Std. Dev.	Voltage
890522	14	24	0.84		0.26	1.11		1.17
890616	12	24	0.88		0.19	1.08		1.14
890701	14	25	0.76		0.13	0.80		1.23
890724	18	24	0.86		0.09	0.88		1.23
890814	15	24	1.18		0.06	0.93		1.23
900522	15	24	1.16	0.20	0.088	0.68	0.20	1.24
900524	15	24	1.03	0.16	0.08	0.87	0.30	1.24
900607	15	24	1.27	0.21	0.08	0.79	0.29	1.32
900626	16	24	0.91	0.13	0.08	0.94	0.34	1.48
900711	10	23	0.98	0.17	0.084	0.99	0.35	1.56
910726	14	22	1.17	0.20	0.08	1.01	0.27	1.21
910730	16	21	0.79	0.10	0.07	0.92	0.36	1.15
910802	19	26	1.16	0.19	0.03	0.74	0.17	1.12
910814	19	23	1.23	0.13	0.08	0.53	0.13	1.12
920508	14	24	0.87	0.03	0.08	0.99	0.09	1.23
920529	13	22	1.07	0.04	0.08	1.21	0.07	1.23
930805	16	22	0.99	0.09	0.08	1.50	0.38	1.23
940430	13	22	0.95	0.04	0.08	1.29	0.07	1.23
940521	12	24	0.95	0.08	0.08	1.26	0.11	1.15
940801	15	25	1.03	0.07	0.08	1.08	0.12	1.10
970625	14	25	1.04	0.16	0.08	0.96	0.27	1.10
990420	12	23	1.00	0.10	0.08	0.98	0.17	1.10

[a]The voltage settings for the discriminator levels used are shown (Discrim. Level).

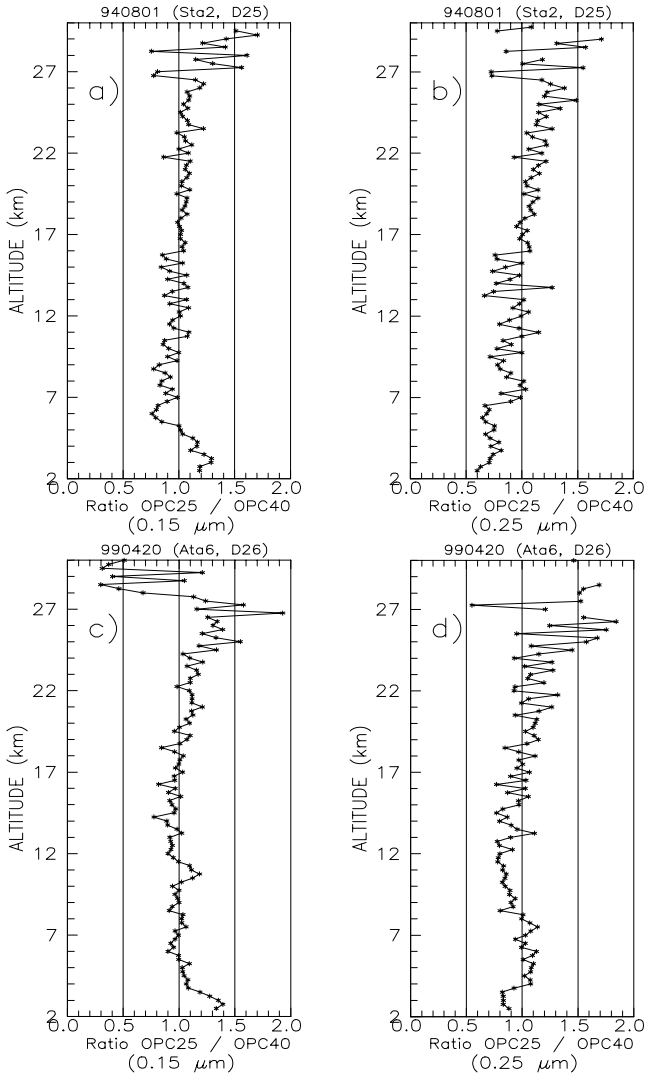

Figure 4. Ratio of aerosol concentrations at 0.15 and 0.25 μm measured with an OPC25 and an OPC40, for measurements in 1994 and 1999. In the stratosphere concentration ratio averages for 0.15 (0.25) μm particles are 1.03 ± 0.07 (1.08 ± 0.12) in 1994 and 1.00 ± 0.10 (0.98 ± 0.17) in 1999.

CN concentration, is obtained when the lower integration limit is set to some low value, say 0.01 μm. $N(>0.01\ \mu m) = N_1 + N_2$ = the CN concentration, which is measured.

[23] The fitting method consists of minimizing the root mean square error = $\Sigma_i \log^2 [N_m(>r_i)/N(>r_i)]$. The summation is over all measured sizes, r_i. $N_m(>r_i)$ is the measured concentration of all particles with $r > r_i$, $N(>r_i)$ is defined by (2). The method consists of trying all combinations of measured concentrations to find the set of discrete sizes plus CN giving size distribution parameters which minimize the root mean square error when all measurements are included. To obtain bimodal distributions requires at a minimum five independent measurements of number concentration. If necessary, the sixth measurement is obtained by setting the concentration, at the first size in which there are no counts, to a value well below the detection limit of the instrument, $\sim 10^{-5}$ cm^{-3} for an OPC40. If there are less than five independent concentration measurements, then a unimodal distribution is applied. This is the case for all OPC25 measurements unless they were supplemented with the 50 L min^{-1} counter mentioned earlier. Unimodal distribution parameters are found in the same way. Example size distributions for measurements at 20 km above Laramie during high aerosol loading following Pinatubo and during the present volcanically quiescent period are shown in Figure 5. The fitted size distributions are not forced to be bimodal. If a unimodal distribution provides a better fit, then that is used instead of a bimodal fit, but this is rarely the case when there are more than four independent measurements.

[24] Lognormal size distributions are used for several reasons. First, these size distributions represent the data well in most cases: see Figure 5. Second, they are easy to use: six parameters specify the complete size distribution, and there are analytical expressions for the distribution moments. Third, there is some experimental basis to expect aerosol populations to evolve into lognormal size distributions [*Granqvist and Buhrman*, 1976]. In most cases, stratospheric aerosol can be classified as aged aerosol. For the time when only the OPC25 and CN counter were flown, serious questions can be raised concerning how well a unimodal lognormal distribution fit to these data represents the true atmospheric aerosol. This is particularly true in periods when large particles are present. Initial attempts to address this problem led to the development of the 50 L min^{-1} counter to provide measurements at radii >1.0 μm, providing 5 size-resolved measurements plus CN [*Hofmann and Rosen*, 1982]. *Rosen and Hofmann* [1986] tested a number of different size distribution models to represent these data, constraining models to provide distribution moments in agreement with independently measured aero-

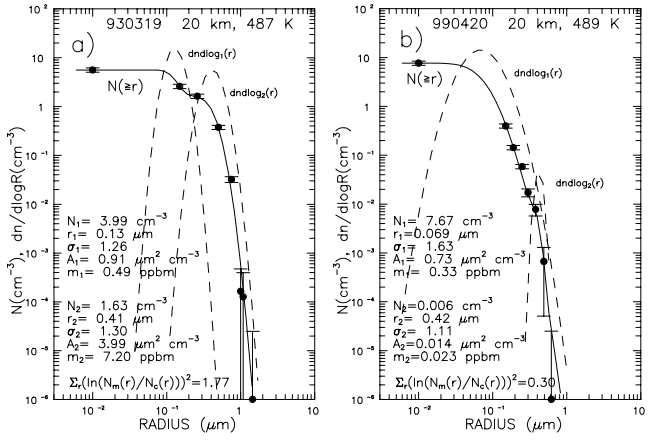

Figure 5. Bimodal lognormal size distributions fit to optical particle counter measurements for (a) a 1993 measurement in volcanic aerosol and (b) a 1999 measurement in background aerosol. The error bars on the measurements (data points) represent the counting uncertainty of the measurement The differential lognormal distributions for each mode are the dashed lines, and the cumulative concentration, from summing the integrals of the differential distributions, is the solid line. The parameters of the size distributions and the inferred surface areas and volumes are shown. The root mean square error of the fit is shown at the bottom.

sol mass and backscatter. While the final model performed well under these constraints, the result was somewhat unsatisfying, a combination of a lognormal distribution at small sizes coupled with a spline function to capture the large particle mode. *Jäger and Hofmann* [1991] elected to fit bimodal lognormal size distributions to these data and used them to calculate conversion factors for lidar backscatter to mass, surface area, and extinction. A similar study on the complete data set was completed by *Jäger and Deshler* [2002].

[25] Monte Carlo simulations are used to assess the impact of measurement uncertainty, due to counting statistics and precision for concentration measurements, and due to pulse width broadening for sizing uncertainties. Random errors applied to this simulation were as follows: for concentration, the maximum of ±10% or the Poisson counting uncertainty; and for radii, uncertainties established by PMT pulse width broadening measurements (∼±10–30% dependent on particle size). Simulations lead to estimates of uncertainties on the parameters of fitted lognormal size distributions and on derived surface areas and volumes. Results of 750 simulations on four example measurements had standard deviations of 20% for distribution width, 30% for median radii, and 40% for surface area and volume. The greatest uncertainties were in determining N_2 in periods of low aerosol loading. In these cases, standard deviations were over 100%. In contrast, under high aerosol loading, N_2 is determined to within 10%.

[26] We conclude that for lognormal size distributions fit to the in situ measurements, surface areas and volumes have uncertainties of ±40%, median radii ±30%, and distribution widths ±20%. These are the population standard deviations from Monte Carlo simulations, and are slightly larger than errors previously quoted [*Deshler et al.*, 1993; *Deshler and Oltmans*, 1998]. An alternate approach using optimal estimation [*Rodgers*, 2000] to fit size distributions to measured concentration data is under study.

5. Laramie Record

[27] Measurements above Laramie began in 1971 with the two channel OPC25. They have continued unabated since that time using several variations on the original instrument. Table 1 provides a history of aerosol sizes measured and instruments used during this thirty year period. While instruments have changed somewhat, measurements at 0.15 and 0.25 μm have been maintained throughout the record. Thus concentration measurements at these sizes provide the best data from this record to investigate changes in stratospheric aerosol over the measurement period. In addition to the Laramie measurements, yearly OPC40 measurements were begun at a conjugate latitude site, Lauder, New Zealand, following the eruption of Pinatubo. More frequent aerosol soundings, begun in 1992 from Lauder using backscattersondes, have been presented by *Liley et al.* [2001]. Figure 6 presents peak aerosol mixing ratios and a ±2 km average around the peak for 1971–2001. Altitudes for the peak mixing ratios averaged 20 km at both sizes with a standard deviation of 2.5 km. Sounding frequency at Laramie is approximately monthly, but there are year to year variations dependent upon volcanic activity and other commitments. The record

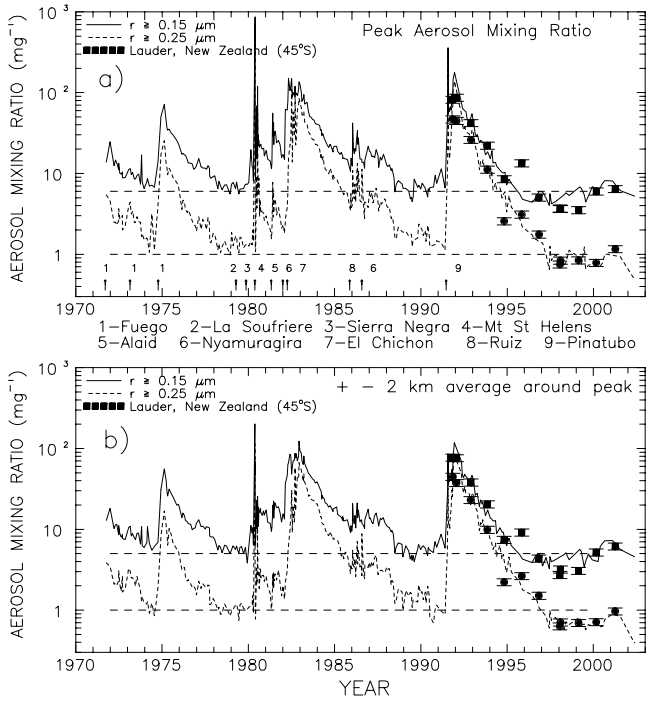

Figure 6. History of aerosol mixing ratios at 0.15 and 0.25 μm from in situ Laramie (41°N) measurements, 1971–2003, and in situ Lauder, New Zealand (45°S), measurements, 1991–2001. The Laramie measurements represent about 340 individual aerosol profiles. The error bars on the Lauder measurements are representative of the Laramie measurements as well. (a) Peak aerosol mixing ratio. (b) 4 km average of aerosol mixing ratio centered on the peak aerosol mixing ratio. The dashed lines are horizontal and are meant only to aid the reader.

shown represents about 340 individual balloon flights. Figure 6 presents data in the form that has appeared in the literature in the past [*Hofmann and Rosen*, 1980; *Hofmann*, 1990]. The dominant impact of volcanic activity on stratospheric aerosol is clearly evident from this figure. While the decay rates during the first two years following Fuego, El Chichón, and Pinatubo are similar, the longer period following El Chichón is interspersed with minor volcanic eruptions. Similar events did not influence recovery following Fuego and Pinatubo.

[28] Also evident in Figure 6 is the change in peak aerosol mixing ratio when comparing 1979 with 1989. Although the mixing ratios of 0.15 μm particles are similar there is an increase in the mixing ratio of 0.25 μm particles. This led *Hofmann* [1990] to the conclusion, discussed earlier, that there may be an increase in stratospheric aerosol mass due to nonvolcanic sources. This difference is maintained when averages around peak mixing ratios are presented in Figure 6b, although there is almost a step change in 0.25 μm averages in late 1990 to early 1991, prior to Pinatubo, and after publication of the work by *Hofmann* [1990]. This difference at 0.25 μm is not maintained when 1979 is compared to the present. Since 1997, particle mixing ratios at both 0.15 and 0.25 μm are at or below the 1979 measurements. The southern hemisphere measurements closely follow Laramie measurements for most comparisons, sug-

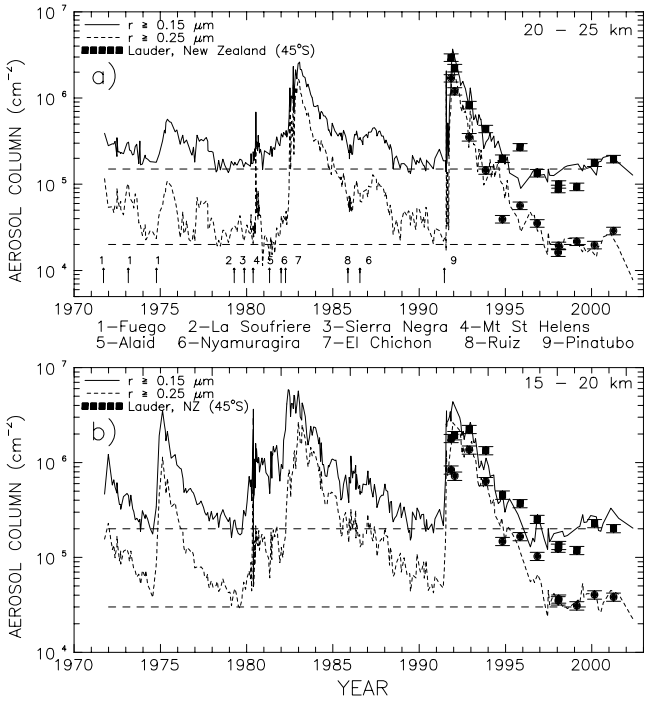

Figure 7. As Figure 6, but for 5 km column integrals of the in situ measurements. (a) 20–25 km and (b) 15–20 km.

gesting significant interhemisphere mixing of stratospheric aerosol, or, at a minimum, similar initial effects and subsequent midlatitude evolution after the tropical Pinatubo eruption.

[29] To provide some altitude resolution, Figure 7 presents 5-km column integrals from 15–20 km and 20–25 km. The pattern is similar to that seen in Figure 6 with some differences. The altitude integrals clearly demonstrate that the impact of Fuego was primarily below 20 km, while El Chichón and Pinatubo produced effects above 25 km. The impact of both El Chichón and Pinatubo was uniform at both sizes measured above 20 km and for Pinatubo above 15 km. The impact of El Chichón below 20 km had some differences at the two sizes, with 0.25 μm particle concentrations lagging the increase in concentration of smaller particles. Clearly, below 20 km the concentration of 0.25 μm particles had not returned to 1979 levels prior to the eruption of Pinatubo. Again the New Zealand measurements follow closely the northern hemisphere measurements, although there are some differences notably around 1996.

[30] Both Figures 6 and 7 suggest that decay of aerosols following Pinatubo has not been impacted by minor volcanic eruptions, and that Pinatubo aerosols were completely removed from the midlatitude stratosphere by early 1997. This has already been concluded from other long-term measurements [*Barnes and Hofmann*, 1997]. The peak aerosol mixing ratios indicate that stratospheric aerosol may have returned to 1979 levels prior to Pinatubo; however, the 5-km column integrals suggest that aerosol concentrations at 0.25 μm did not reach pre-El Chichón levels prior to Pinatubo below 20 km.

[31] The final 0.25 μm measurement shown in Figures 6 and 7 is intriguing. The instrument used performs two independent measurements at 0.25 μm, and the two measurements agreed to within experimental error. The suggestion of possibly additional decreases for aerosol >0.25 μm, particularly above 20 km, is, however, based on a single aerosol profile in May 2002 and is premature.

[32] At Lauder, CN were measured simultaneously with aerosol ≥0.15 μm in 1998, 2000, and 2001. For all other years, CN measurements from the Laramie record were used when fitting size distributions to the Lauder data. A comparison of the CN profiles in 1998, 2000, and 2001 between Lauder and Laramie suggests this is a reasonable substitution. Between 15 and 25 km, CN profiles from Laramie matched quite closely the Lauder profiles measured. The largest differences of 25% occurred between 20 and 25 km.

[33] Once size distributions are established for size resolved aerosol concentration measurements, any size distribution moment including aerosol surface area, volume, and extinction can be easily calculated. Calculated extinctions from Laramie size distributions have been compared with visible and near infrared wavelengths of SAGE II and infrared measurements of HALOE [*Hervig et al.*, 1996; *Hervig and Deshler*, 2002]. In general, calculated and measured extinctions are in agreement to within about 50% for SAGE II and HALOE, with additional discrepancies at some wavelengths in periods of low aerosol loading. Five-kilometer column integrals of aerosol extinction at 386 and 452 nm calculated from Laramie in situ measurements are compared with SAGE II measurements in Figure 8. The agreement is in general reasonable except just before Pinatubo and the present. The comparison in Figure 8, using SAGE II version (v) 6.1 data, is somewhat worse than presented by *Hervig and Deshler* [2002], who compared the in situ measurements to SAGE II v6.0 data. This results from an increase in aerosol extinction at low aerosol loading at the shorter wavelengths in v6.1 compared with v6.0. There is almost no change in the v6.1 1020 nm extinctions.

[34] Aerosol surface areas and volumes can in turn be calculated from both SAGE II and HALOE [*Thomason et al.*, 1997b; *Hervig et al.*, 1998]. SAGE II surface areas and volumes are calculated using principal component analysis [*Twomey*, 1977; *Thomason and Poole*, 1993; *Steele et al.*, 1999]. Figure 9 compares two of the longest records of stratospheric aerosol surface area available. The SAGE II aerosol moments were obtained from the SAGE II database. No significant difference was found between these moments and moment calculations using the SAGE II extinctions following *Steele et al.* [1999]. The SAGE II data are averaged over a ±10° longitude and ±1° latitude bin centered on Laramie, without any restriction on time. The agreement between the two data sets is surprisingly good, well within the measurement precision from the two data sets over most of the record. Differences appear primarily during periods of low aerosol loading such as the present and just prior to Pinatubo, with the differences in surface areas somewhat greater than the differences in aerosol volume. The SAGE II surface areas are centered at the base of the error bars on the Laramie measurements, particularly noticeable since 1997. This difference was greater when the in situ measurements were compared with v6.0 SAGE II data (not shown) [*Hervig and Deshler*, 2002]. This difference did not appear in comparisons by *Thomason et al.* [1997b], but that analysis did not extend to the present background period.

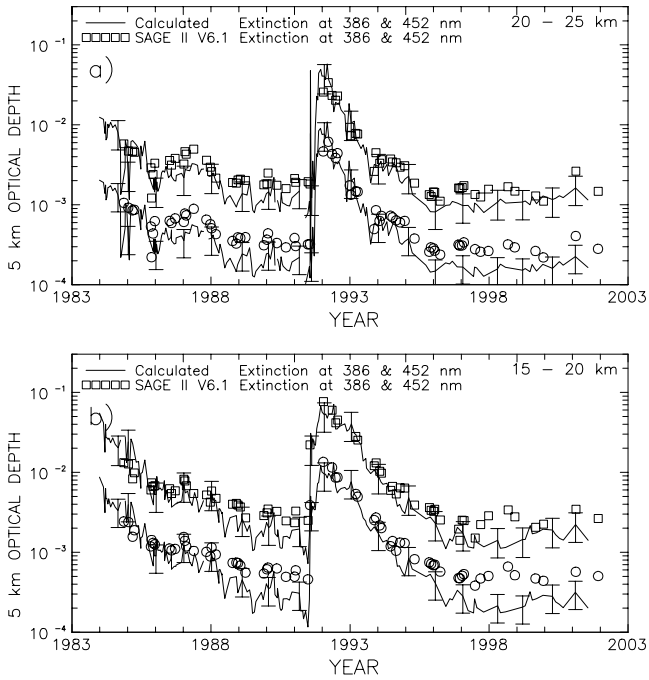

Figure 8. Five kilometer column integrals of aerosol extinction at 386 and 452 nm from SAGE II version 6.1 measurements (symbols) and calculated from in situ size distributions measurements from Laramie (lines). The SAGE II data are from a ±10° longitude and ±1° latitude bin centered on Laramie. The 452 nm comparison has been artificially lowered by a factor of 5 for clarity. Error bars on the occasional Laramie measurement reflect the ±40% error discussed in the text.

[35] The change from SAGE II v6.0 to v6.1 data led to a larger difference with in situ extinctions, but a smaller difference with in situ surface area. The higher v6.1 extinctions increase the surface area estimates bringing the surface area estimates closer to the in situ measurements. A similar comparison with aerosol surface areas inferred from the Polar Ozone and Aerosol Measurement (POAM) instrument has not been made because of the latitude coverage of the latter instrument; however, a comparison of POAM II, III, and SAGE II aerosol surface areas [*Randall et al.*, 2000, 2001] suggests that a similar discrepancy between in situ and POAM estimates of aerosol surface area may exist. The magnitude of the discrepancy, however, would probably be less, particularly if compared with POAM III which has surface area estimates ~30% greater than SAGE II surface area estimates. POAM II is closer to the SAGE II estimates. *Steele et al.* [1999] predicted differences in surface areas of this magnitude between the two instruments in background conditions when the aerosol are small. These results do not support the reduction in SAGE II estimates of aerosol surface areas used by *Fish et al.* [2000] to bring calculated NO_2 trends more in line with observations.

[36] An explanation for the disparity in surface areas at low aerosol loading is offered in Figure 10. Differential surface area, volume, and extinction distributions are compared for measurements at two altitudes in 1993, under high aerosol loading, and measurements at two altitudes in 1999, under low aerosol loading. For the comparison of differential extinction and volume distributions, Figures 10a and 10b, similar aerosol sizes are important for both distributions. Thus a measurement of extinction is a good approximation to a measurement of aerosol volume, appropriately rescaled. Figures 10a and 10b clearly show the importance of the second mode of the aerosol size distribution in 1993, and its less important, but still notable, contribution in 1999. The similarity of differential volume and extinction distributions does not carry over to the comparisons of extinction and surface area, Figures 10c and 10d. In this case there is proportionality at high aerosol loading in 1993, but not at low aerosol loading such as in 1999 and the present. Even in 1993 the extinction distribution only spans part of the distribution important for surface area, but it spans the most important contribution in the second mode of the distribution, thus again a measurement of extinction can provide a reasonable estimate of surface area. Under low aerosol loading this is not the case. The median radius of the surface area distribution is either completely below the tail of the extinction distribution, as at 15 km, or near the tail of the distribution, at 20 km. At 15 km this is a factor of 2 below the peak of the extinction distribution. In contrast to the volume distributions, where even under low aerosol loading, the second mode makes a significant contribution to the total volume, for surface area the second mode is much less important.

[37] Figures 10c and 10d illustrate the difficulty to be encountered when using extinction measurements, sensitive

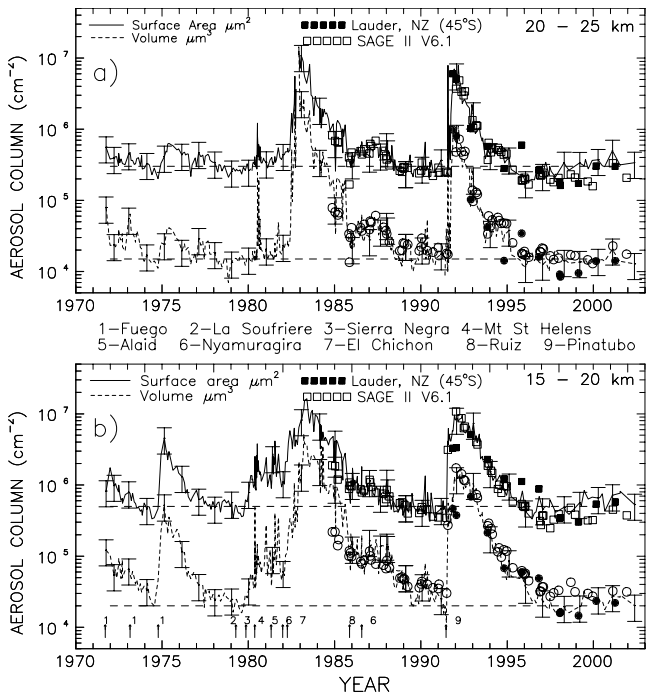

Figure 9. As Figure 6, but for aerosol surface area and volume concentrations. The error bars, representing the ±40% uncertainty discussed in the text, are shown for occasional Laramie measurements. SAGE II version 6.1 estimates of aerosol surface area (open boxes) and volume (open circles), 1984–2002, are available on the SAGE II web site. Uncertainties on the SAGE II measurements are given as ±30%.

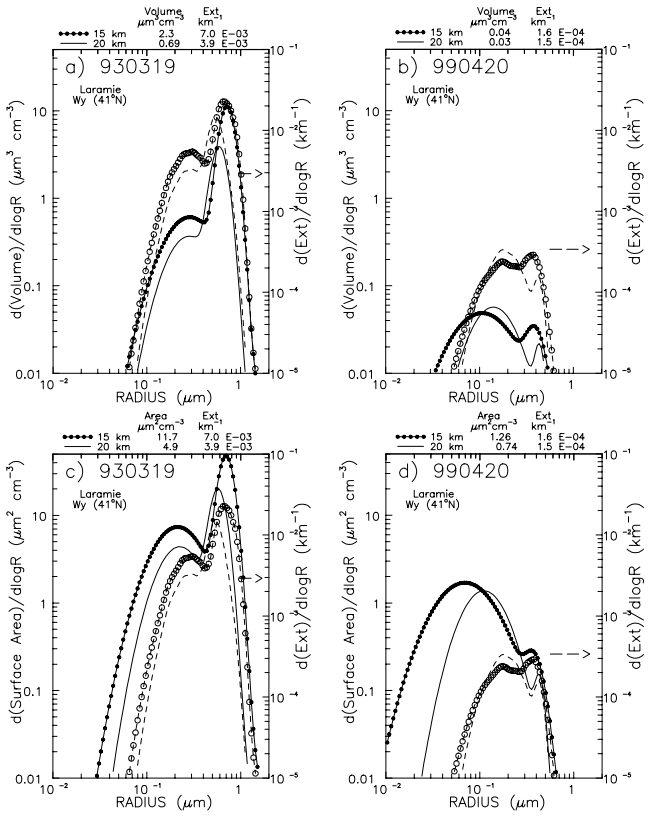

Figure 10. Differential distributions at 15 (symbols) and 20 (lines) km for extinction, volume, and surface area for volcanic aerosol (930319) and background aerosol (990420). Extinction is given by open symbols, dashed lines, and scale on the left, while volume and surface area by closed symbols, solid lines, and scale on the right. (a) Volume and extinction on 930319, (b) volume and extinction on 990420, (c) surface area and extinction on 930319, and (d) surface area and extinction on 990420.

to particles between 0.05 and 0.5 μm, to infer aerosol surface area, when the latter moment is controlled by particles between 0.01 and 0.5 μm, and half of the distribution is below 0.05 μm. Accurate measurements of aerosol surface areas under these conditions, even from the in situ measurements discussed here, are also problematic since the dominant mode of the distribution is captured by just three measurements: CN, and aerosol >0.15 and >0.25 μm; and the latter two only fix the tail of the distribution and are well above the inferred median radius. To obtain more accurate measurements will require size-resolved concentration measurements between 0.01 and 0.1 μm. Present aircraft instruments are capable of this with size-resolved measurements for particles >0.03 μm [*Jonsson et al.*, 1995], but resolution of particle sizes below 0.15 μm from balloon-borne platforms will have to await instruments now in the planning stage.

6. Summary and Conclusions

[38] There are only a few long-term stratospheric aerosol records. These include lidar records at Garmisch-Partenkirchen, Germany [*Jäger*, 1991], Hampton, Virginia [*Osborn et al.*, 1995], and Mauna Loa, Hawaii [*Barnes and Hofmann*, 1997], satellite records from SAGE II [*Thomason et al.*, 1997b] and in situ balloon-borne measurements at Laramie, Wyoming. This latter record spans the period 1971–2001, making it the longest continuous record available. Although there have been a few instrument changes during this period, care has been exercised to insure that all instrument changes provide continuity of the fundamental measurements, aerosol with radius ≥0.15, 0.25 μm and CN.

[39] The techniques underlying the preparation and application of the balloon-borne in situ instruments flown from Laramie have been reviewed. The instruments are calibrated with monodisperse aerosol using standard techniques. Uncertainties in aerosol concentration measurements are dependent on Poisson counting statistics and range from ±85% at 0.001 (0.01) cm^{-3} to ±10% at 0.1 (1.0) cm^{-3} for the high (low) flow rate counter. Uncertainties in aerosol size, due primarily to pulse width broadening, are on the order of 10%. The impacts of these uncertainties on inferred bimodal lognormal aerosol size distributions and their moments are on the order of ±20–30% for lognormal parameters, and ±40% for aerosol surface area and volume concentrations. A fundamental instrument change was undertaken in the early 1990s. Comparisons of the new and old instrument are presented. Present midlatitude capability is to measure CN and aerosol with radius ≥0.15–2.0 μm in twelve size bins.

[40] Thirty years of measurements at Laramie (41°N) and ten years at Lauder, New Zealand (45°S), are presented in terms of peak aerosol mixing ratios and 15–20 and 20–25 km column integrals. The southern hemisphere measurements were made with Wyoming instruments as well, and with a few exceptions provide a striking agreement for measurements from the two sites. The 1971–2001 record clearly illustrates how volcanic activity dominates the aerosol record during this period. Three major eruptions, Fuego, El Chichón, and Pinatubo, with a few minor eruptions in the late 1970s and early and mid 1980s, have caused nearly 20 of the past 30 years to be dominated by enhancement from volcanic emissions. This is in contrast to the period prior to the beginning of the modern measurement records in the 1970s. *Junge*'s [1961] initial measurements of stratospheric aerosol were at the tail of a volcanically quiescent period which had extended from the 1920s [*Stothers*, 1996]. Within the modern record, the present volcanically quiescent period, since 1997, represents the longest such quiet period. These midlatitude data suggest that there have not been significant changes in aerosol loading under background conditions over the past 30 years. See also *Barnes and Hofmann* [1997, 2001].

[41] Inferred aerosol surface areas and volumes from the in situ measurements and from SAGE II are compared for the period from 1984–2000. The agreement between these two independent measurements, with no tuning of one measurement to the other, is within measurement uncertainty for aerosol volume for both volcanic and background aerosol. The same is true for surface area of volcanic aerosol, but for background aerosol the SAGE II surface areas are about 40% low. In the latter case a comparison of differential surface area and extinction distributions indicates that in background conditions aerosol sizes which control surface

area distributions are primarily below those which control extinction, thus visible extinction measurements may provide a poor representation for surface area, tending to underestimate it. The same is not true for volume. Sizes which contribute to volume and extinction are similar, thus extinction can be scaled to give a good estimate of volume.

[42] Even though local in situ and remote measurements of stratospheric aerosol can never provide the global coverage essential for the incorporation of stratospheric aerosol data into global chemical and radiation models, they do provide long-term continuity, more accurate estimates of some aerosol parameters, and important checks on remote global satellite data. Local long term lidar and in situ measurement records will continue to have an important role to play in deepening our understanding of the chemical and radiative balance of the Earth's atmosphere. The long term Laramie aerosol record is unique in providing a thirty-year record of altitude-resolved aerosol size distribution data. These data at 0.5 and 1.0 km vertical intervals are available to the community. See www-das.uwyo.edu/~deshler for the ftp address.

[43] **Acknowledgments.** These measurements over the years have been supported by the National Science Foundation, the National Aeronautics and Space Administration, and the Office of Naval Research. The most recent support has also been from the National Science Foundation. Many individuals at the University of Wyoming have contributed to the quality and the longevity of these measurements, and we acknowledge their hard work and willingness to spend many an early morning on the Laramie plains waiting for the winds to fall to favorable levels for a launch. These include G. Olson, N. Kjome, L. Womack, J. Gonzales, B. Johnson, B. Nardi, and C. Kröger, and at Lauder, B. McNamara, J. Robinson, S. Wood, and K. Kreher.

References

Angell, J. K., Comparisons of stratospheric warming following Agung, El Chichón, and Pinatubo volcanic eruptions, *Geophys. Res. Lett.*, *20*, 715–718, 1993.

Angell, J. K., J. Korshover, and W. G. Planet, Ground-based and satellite evidence for a pronounced total-ozone minimum in early 1983 and responsible atmospheric layers, *Mon. Weather Rev.*, *113*, 641–646, 1985.

Barnes, J. E., and D. J. Hofmann, Lidar measurements of stratospheric aerosol over Mauna Loa, *Geophys. Res. Lett.*, *24*, 1923–1926, 1997.

Barnes, J. E., and D. J. Hofmann, Variability in the stratospheric background aerosol over Mauna Loa observatory, *Geophys. Res. Lett.*, *28*, 2895–2898, 2001.

Crutzen, P. J., The influence of nitrogen oxide on the atmospheric ozone content, *Q. J. R.. Meteorol. Soc.*, *96*, 320–327, 1970.

DeFoor, J. E., E. Robinson, and S. Ryan, Early lidar measurements of the June 1991 Pinatubo eruption plume at Manua Loa Observatory, Hawaii, *Geophys. Res. Lett.*, *19*, 187–190, 1992.

Deshler, T., and S. J. Oltmans, Vertical profiles of volcanic aerosol and polar stratospheric clouds above Kiruna, Sweden: Winters 1993 and 1995, *J. Atmos. Chem.*, *30*, 11–23, 1998.

Deshler, T., B. J. Johnson, and W. R. Rozier, Balloonborne measurements of Pinatubo aerosol during 1991 and 1992 at 41°N, vertical profiles, size distribution, and volatility, *Geophys. Res. Lett.*, *20*, 1435–1438, 1993.

Deshler, T., B. J. Johnson, D. J. Hofmann, and B. Nardi, Correlations between ozone loss and volcanic aerosol at latitudes below 14 km over McMurdo Station, Antarctica, *Geophys. Res. Lett.*, *23*, 2931–2934, 1996.

Dutton, E. G., and J. R. Christy, Solar radiative forcing at selected locations and evidence for global lower tropospheric cooling following the eruptions of El Chichón and Pinatubo, *Geophys. Res. Lett.*, *19*, 2313–2316, 1992.

Fahey, D. W., et al., In situ measurements constraining the role of sulphate aerosols in mid-latitude ozone depletion, *Nature*, *363*, 509–514, 1993.

Fish, D. J., H. K. Roscoe, and P. V. Johnston, Possible causes of stratospheric NO_2 trends observed at Lauder, New Zealand, *Geophys. Res. Lett.*, *27*, 3313–3316, 2000.

Gleason, J. F., et al., Record low global ozone in 1992, *Science*, *260*, 523–526, 1993.

Grainger, R. G., A. Lambert, C. D. Rodgers, F. W. Taylor, and T. Deshler, Stratospheric aerosol effective radius, surface area, and volume estimated from infrared measurements, *J. Geophys. Res.*, *100*, 16,507–16,518, 1995.

Granqvist, C. G., and R. A. Buhrman, Log-normal size distributions of ultrafine metal particles, *Solid State Commun.*, *18*, 123–126, 1976.

Gruner, P., and H. Kleinert, Die dammerungerscheinen, *Probl. Kosm. Phys.*, *10*, 1–113, 1927.

Hayashida, S., and M. Horikawa, Anti-correlation between stratospheric aerosol extinction and the Ångström parameter from multiple wavelength measurements with SAGE II - a characteristic of the decay period following major volcanic eruptions, *Geophys. Res. Lett.*, *28*, 4063–4066, 2001.

Hervig, M. E., and T. Deshler, Evaluation of aerosol measurements from SAGE II, HALOE, and balloon-borne optical particle counters, *J. Geophys. Res.*, *107*(D3), doi:10.1029/2001JD000703, 2002.

Hervig, M. E., J. M. Russell III, L. L. Gordley, J. H. Park, S. R. Drayson, and T. Deshler, Validation of aerosol measurements made by the Halogen Occultation Experiment, *J. Geophys. Res.*, *101*, 10,267–10,276, 1996.

Hervig, M. E., T. Deshler, and J. M. Russell III, Aerosol size distributions obtained from HALOE spectral extinction measurements, *J. Geophys. Res.*, *103*, 1573–1583, 1998.

Hofmann, D. J., Increase in the stratospheric background sulfuric acid aerosol mass in the past 10 years, *Science*, *248*, 996–1000, 1990.

Hofmann, D. J., and T. Deshler, Stratospheric cloud observations during formation of the Antarctic ozone hole in 1989, *J. Geophys. Res.*, *96*, 2897–2912, 1991.

Hofmann, D. J., and J. M. Rosen, Stratospheric sulfuric acid layer: Evidence for an anthropogenic component, *Science*, *208*, 1368–1370, 1980.

Hofmann, D. J., and J. M. Rosen, On the background stratospheric aerosol layer, *J. Atmos. Sci.*, *38*, 168–181, 1981a.

Hofmann, D. J., and J. M. Rosen, Stratospheric aerosol and condensation nuclei enhancements following the eruption of Alaid in April 1981, *Geophys. Res. Lett.*, *8*, 1231–1234, 1981b.

Hofmann, D. J., and J. M. Rosen, Balloon-borne observations of stratospheric aerosol and condensation nuclei during the year following the Mt. St. Helens eruption, *J. Geophys. Res.*, *87*, 11,039–11,061, 1982.

Hofmann, D. J., and J. M. Rosen, Sulfuric acid droplet formation and growth in the stratosphere after the 1982 eruption of El Chichón, *Science*, *222*, 325–327, 1983.

Hofmann, D. J., and J. M. Rosen, Measurement of the sulfuric acid weight percent in the stratospheric aerosol from the El Chichón eruption, *Geofis. Int.*, *23*, 309–320, 1984.

Hofmann, D. J., and J. M. Rosen, On the prolonged lifetime of the El Chichón sulfuric acid aerosol cloud, *J. Geophys. Res.*, *92*, 9825–9830, 1987.

Hofmann, D. J., and S. Solomon, Ozone destruction through heterogeneous chemistry following the eruption of El Chichón, *J. Geophys. Res.*, *94*, 5029–5041, 1989.

Hofmann, D. J., J. M. Rosen, T. J. Pepin, and R. G. Pinnick, Stratospheric aerosol measurements, I, Time variations at nothern midlatitudes, *J. Atmos. Sci.*, *32*, 1446–1456, 1975.

Jäger, H., Stratospheric aerosols: Observations, trends, and effects, *J. Aerosol Sci.*, *22*, suppl. 1, S517–S520, 1991.

Jäger, H., and T. Deshler, Lidar backscatter to extinction, mass and area conversions for stratospheric aerosols based on midlatitude balloonborne size distribution measurements, *Geophys. Res. Lett.*, *29*(19), 1929, doi:10.1029/2002GL015609, 2002.

Jäger, H., and D. J. Hofmann, Midlatidude lidar backscatter to mass, area, and extinction conversion model based on in situ aerosol measurements from 1980 to 1987, *Appl. Opt.*, *30*, 127–138, 1991.

Jäger, H., and K. Wege, Stratospheric ozone depletion at northern midlatitudes after major volcanic eruptions, *J. Atmos. Chem.*, *10*, 273–287, 1990.

Johnston, P. V., and R. L. McKenzie, NO_2 observatins at 45°S during the decreasing phase of solar cycle 21, from 1980 to 1987, *J. Geophys. Res.*, *94*, 3473–3486, 1989.

Johnston, P. V., R. L. McKenzie, J. G. Keys, and W. A. Matthews, Observations of depleted stratospheric NO_2 following the Pinatubo volcanic eruption, *Geophys. Res. Lett.*, *19*, 211–213, 1992.

Jonsson, H. H., et al., Performance of a focused cavity aerosol spectrometer for measurements in the stratosphere of particle size in the 0.06–2.0 μm diameter range, *J. Oceanic Atmos. Technol.*, *12*, 115–129, 1995.

Junge, C. E., C. W. Changnon, and J. E. Manson, Stratospheric aerosols, *J. Meteorol*, *18*, 81–108, 1961.

Labitzke, K., and M. P. McCormick, Stratospheric temperature increases due to Pinatubo aerosols, *Geophys. Res. Lett.*, *19*, 207–210, 1992.

Lambert, A., R. G. Grainger, J. J. Remedios, W. J. Reburn, C. D. Rodgers, F. W. Taylor, A. E. Roche, J. B. Kumer, S. J. Massie, and T. Deshler, Validation of aerosol measurements from the improved stratospheric and mesospheric sounder, *J. Geophys. Res.*, *101*, 9811–9830, 1996.

Liley, J. B., J. M. Rosen, N. T. Kjome, N. P. Jone, and C. P. Rinsland, Springtime enhancement of upper tropospheric aerosol at 45°S, *Geophys. Res. Lett.*, *28*, 1495–1498, 2001.

Massie, S. T., et al., Validation studies using multiwavelength Cryogenic Limb Array Etalon Spectrometer (CLAES) observations of stratospheric aerosol, *J. Geophys. Res.*, *101*, 9757–9774, 1996a.

Massie, S. T., T. Deshler, G. E. Thomas, J. L. Mergenthaler, and J. M. Russell, Evolution of the infrared properties of the Mt. Pinatubo aerosol cloud over Laramie, Wyoming, *J. Geophys. Res.*, *101*, 23,007–23,020, 1996b.

McCormick, M. P., P. Hamill, T. J. Pepin, W. P. Chu, T. J. Swissler, and L. R. McMaster, Satellite studies of the stratospheric aerosol, *Bull. Am. Meteorol. Soc.*, *60*, 1038–1046, 1979.

McCormick, M. P., L. W. Thomason, and C. R. Trepte, Atmospheric effects of the Mt. Pinatubo eruption, *Nature*, *373*, 399, 1995.

Miao, Q., An analysis of errors associated with the measurement of aerosol concentration in situ with optical particle counters, M. S. thesis, 71 pp., Univ. of Wyo., Laramie, 2001.

Mozurkiewicz, M., and J. G. Calvert, Reaction probability of N_2O_5 on aqueous aerosols, *J. Geophys. Res.*, *93*, 15,889–15,896, 1988.

Oesburg, F., The influence of the aperture on the optical system of aerosol particle counters on the response curve, *J. Aerosol Sci.*, *3*, 307–311, 1972.

Osborn, M. T., R. J. DeCoursey, C. R. Trepte, D. M. Winder, and D. C. Woods, Evolution of the Pinatubo volcanic cloud over Hampton, Virginia, *Geophys. Res. Lett.*, *22*, 1101–1104, 1995.

Pepin, T. J., M. P. McCormick, W. P. Chu, F. Simon, T. J. Swissler, R. R. Adams, K. R. Crumbly, and W. H. Fuller Jr., Stratospheric aerosol measurements, *NASA Spec. Publ.*, *SP-421*, 127–136, 1977.

Pinnick, R. G., and D. J. Hofmann, Efficiency of light-scattering aerosol particle counters, *Appl. Opt.*, *12*, 2593–2597, 1973.

Pinnick, R. G., J. M. Rosen, and D. J. Hofmann, Measured light scattering properties of individual aerosol particles compared to Mie scattering theory, *Appl. Opt.*, *12*, 37–41, 1973.

Poole, L. R., and M. C. Pitts, Polar stratospheric cloud climatology based on Stratospheric Aerosol Measurement II observations from 1978 to 1989, *J. Geophys. Res.*, *99*, 13,083–13,089, 1994.

Prather, M. J., Catastrophic loss of stratospheric ozone in dense volcanic clouds, *J. Geophys. Res.*, *97*, 10,187–10,191, 1992.

Quenzel, H., Influence of refractive index on the accuracy of size determination of aerosol particles with light scattering aerosol counters, *Appl. Opt.*, *8*, 165–169, 1969.

Randall, C. E., R. M. Bevilacqua, J. D. Lumpe, K. W. Hoppel, D. W. Rusch, and E. P. Shettle, Comparison of Polar Ozone and Aerosol Measurement (POAM) II and Stratospheric Aerosol and Gas Experiment (SAGE) II aerosol measurements from 1994 to 1996, *J. Geophys. Res.*, *105*, 3929–3942, 2000.

Randall, C. E., R. M. Bevilacqua, J. D. Lumpe, and K. W. Hoppel, Vlaidation of POAM III aerosols: Comparison to SAGE II and HALOE, *J. Geophys. Res.*, *106*, 27,525–27,536, 2001.

Rodgers, C. D., *Inverse Methods for Atmospheric Sounding: Theory and Practice*, World Sci., River Edge, N. J., 2000.

Rosen, J. M., The vertical distribution of dust to 30 km, *J. Geophys. Res.*, *69*, 4673–4676, 1964.

Rosen, J. M., The boiling point of stratospheric aerosols, *J. Appl. Meteorol.*, *10*, 1044–1046, 1971.

Rosen, J. M., and D. J. Hofmann, Balloonborne measurements of condensation nuclei, *J. Appl. Meteorol.*, *16*, 56–62, 1977.

Rosen, J. M., and D. J. Hofmann, Optical modeling of stratospheric aerosols: Present status, *Appl. Opt.*, *25*, 410–419, 1986.

Rosen, J. M., D. J. Hofmann, and K. H. Kaselau, Vertical profiles of condensation nuclei, *J. Appl. Meteorol.*, *17*, 1737–1740, 1978.

Rowland, F. S., H. Sato, H. Khwaja, and S. M. Elliott, The hydrolysis of chlorine nitrate and its possible atmospheric significance, *J. Phys. Chem.*, *90*, 1985–1988, 1986.

Rozier, W. R., Analysis of a balloonborne, continuous flow condensation nuclei growth chamber, M. S. thesis, 57 pp., Univ. of Wyo., Laramie, 1993.

Russell, P. B., and P. Hamill, Spatial variation of stratospheric aerosol acidity and model refractive index: Implications of recent results, *J. Atmos. Sci.*, *41*, 1781–1790, 1984.

Russell, P. B., et al., Satellite and correlative measurements of the stratospheric aerosol, II, Comparison of measurements made by SAM II, dustsondes, and an airborne lidar, *J. Atmos. Sci.*, *38*, 1296–1312, 1981.

Russell, P. B., M. P. McCormick, T. J. Swissler, J. M. Rosen, D. J. Hofmann, and L. R. McMaster, Satellite and correlative measurements of the stratospheric aerosol, III, Comparison of measurements made by SAM II, SAGE, dustsondes, filters, impactors, and lidar, *J. Atmos. Sci.*, *41*, 1792–1800, 1984.

Russell, P. B., et al., Pinatubo and pre-Pinatubo optical-depth spectra: Mauna Loa measurements, comparisons, inferred particle size distributions, radiative effects, and relationship to lidar data, *J. Geophys. Res.*, *98*, 22,969–22,985, 1993.

Russell, P. B., et al., Global to microscale evolution of the Pinatubo volcanic aerosol, derived from diverse measurements and analyses, *J. Geophys. Res.*, *101*, 18,745–18,763, 1996.

Sato, M., J. E. Hansen, M. P. McCormick, and J. B. Pollack, Stratospheric aerosol optical depths, 1850–1990, *J. Geophys. Res.*, *98*, 22,987–22,994, 1993.

Solomon, S., Stratospheric ozone depletion: A review of concepts and theory, *Rev. Geophys.*, *37*, 275–316, 1999.

Solomon, S., R. R. Garcia, F. S. Rowland, and D. J. Wuebbles, On the depletion of Antarctic ozone, *Nature*, *321*, 755–758, 1986.

Solomon, S., R. W. Portmann, R. R. Garcia, L. W. Thomason, L. R. Poole, and M. P. McCormick, The role of aerosol variations in anthropogenic ozone depletion at northern midlatitudes, *J. Geophys. Res.*, *101*, 6713–6727, 1996.

Steele, H. M., and P. Hamill, Effect of temperature and humidity on the growth and optical properties of sulfuric acid-water droplets in the stratosphere, *J. Aerosol Sci.*, *12*, 517–528, 1981.

Steele, H. M., J. D. Lumpe, R. P. Turco, R. M. Bevilacqua, and S. T. Massie, Retrieval of aerosol surface area and volume densities from extinction measurements: Application to POAM II and SAGE II, *J. Geophys. Res.*, *104*, 9325–9336, 1999.

Stevermer, A. J., I. V. Petropavlovskikh, J. M. Rosen, and J. J. DeLuisi, Development of a global stratospheric aerosol climatology: Optical properties and applications for UV, *J. Geophys. Res.*, *105*, 22,763–22,776, 2000.

Stothers, R. B., Major optical depth perturbations to the stratosphere from volcanic eruptions: Pyrheliometric period, 1881–1960, *J. Geophys. Res.*, *101*, 3901–3920, 1996.

Sugita, T., Y. Kondo, M. Koike, M. Kanada, N. Toriyama, H. Nakajima, T. Deshler, and R. Imasu, Balloon-borne optical counter for in situ aerosol measurements, *J. Atmos. Chem.*, *32*, 183–204, 1999.

Thomason, L. W., and L. R. Poole, Use of stratospheric aerosol properties as diagnostics of Antarctic vortex properties, *J. Geophys. Res.*, *98*, 23,003–23,012, 1993.

Thomason, L. W., G. S. Kent, C. R. Trepte, and L. R. Poole, A comparison of the stratospheric aerosol background periods of 1979 and 1989–1991, *J. Geophys. Res.*, *102*, 3611–3616, 1997a.

Thomason, L. W., L. R. Poole, and T. Deshler, A global climatology of stratospheric aerosol surface area density deduced from Stratospheric Aerosol and Gas Experiment II measurements: 1984–1994, *J. Geophys., Res.,102*, 8967–8976, 1997b.

Tolbert, M. A., M. J. Rossi, and D. M. Golden, Heterogeneous interactions of chlorine nitrate, hydrogen chloride, and nitric acid with sulfuric acid surfaces at stratospheric temperatures, *Geophys. Res. Lett.*, *15*, 847–850, 1988.

Twomey, S. A., *Introduction to the Mathematics of Inversion in Remote Sensing Indirect Measurements*, 243 pp., Elsevier Sci., New York, 1977.

Wang, P. H., et al., SAGE II aerosol data validation based on retrieved aerosol model size distribution from SAGE II aerosol measurements, *J. Geophys. Res.*, *94*, 8381–8393, 1989.

Wennberg, P. O., et al., Removal of stratospheric O_3 by radicals: In situ measurements of OH, HO_2, NO, NO_2, ClO, and BrO, *Science*, *266*, 398–404, 1994.

Zhao, R., Laboratory measurements of the response of optical particle counters to particles of different shape and refractive index, 57 pp., M. S. thesis, Univ. of Wyo., Laramie, 1996.

T. Deshler, Department of Atmospheric Science, University of Wyoming, Laramie, WY 82071, USA. (deshler@uwyo.edu; ckroger@uwyo.edu)

M. E. Hervig, GATS Inc., 65 South Main St., Driggs, ID 83422, USA. (m.e.hervig@gats-inc.com)

D. J. Hofmann, National Oceanic and Atmospheric Administration, Boulder, CO 80305, USA. (David.J.Hofmann@noaa.gov)

J. B. Liley, National Institute of Water and Atmospheric Research, Private Bag 50061, Omakau, Lauder, Central Otago, New Zealand. (b.liley@niwa.cri.nz)

J. M. Rosen, Department of Physics and Astronomy, University of Wyoming, Laramie, WY 82071, USA. (wyojim@igc.apc.org)